Evolution towards simplicity in bacterial small heat shock protein system

Piotr Karaś, Klaudia Kochanowicz, Marcin Pitek, Przemyslaw Domanski, Igor Obuchowski, Bartlomiej Tomiczek*, Krzysztof Liberek*

Intercollegiate Faculty of Biotechnology UG-MUG, University of Gdansk, Abrahama 58, 80-307 Gdansk, Poland

*Correspondence to B.T. (bartlomiej.tomiczek@biotech.ug.edu.pl) or K.L. (krzysztof.liberek@ug.edu.pl)

Abstract

Evolution can tinker with multi-protein machines and replace them with simpler single-protein systems performing equivalent functions in equally efficient manner. It is unclear how, on a molecular level, such simplification can arise. With ancestral reconstruction and biochemical analysis we have traced the evolution of bacterial small heat shock proteins (sHsp), which help to refold proteins from aggregates using either two proteins with different functions (IbpA and IbpB) or a secondarily single sHsp that performs both functions in an equally efficient way. Secondarily single sHsp evolved from IbpA, an ancestor specialized in strong substrate binding. Evolution of an intermolecular binding site drove the alteration of substrate binding properties, as well as formation of higher-order oligomers. Upon two mutations in the α-crystallin domain, secondarily single sHsp interacts with aggregated substrates less tightly. Paradoxically, less efficient binding positively influences the ability of sHsp to stimulate substrate refolding, since the dissociation of sHps from aggregates is required to initiate Hsp70-Hsp100-dependent substrate refolding. After the loss of a partner, IbpA took over its role in facilitating the sHsp dissociation from an aggregate by weakening the interaction with the substrate, which became beneficial for the refolding process. We show that the same two amino acids introduced in modern-day system define whether the IbpA acts as a single sHsp or obligatorily cooperates with an IbpB partner. Our discoveries illuminate how one sequence has evolved to encode functions previously performed by two distinct proteins.

Introduction

Gene birth and loss is a hallmark of protein family evolution, however molecular determinants and genetic mechanisms enabling that process are not well understood (Fernandez & Gabaldon, 2020; Iranzo *et al*, 2019). In complex protein systems execution of a cellular function can be shared between several proteins. In bacteria the cost of maintaining additional gene copy is very high and maintaining low gene count is important for keeping the replication energy costs low (Kempes *et al*, 2017; Lever *et al*, 2015; Lynch & Marinov, 2015). Still, it remains unclear how a multi-protein system can undergo simplification. Here we asked what are the molecular events that enabled the gene loss, and how one of the biochemical functions has been taken over by the other protein. We investigated these questions using small heat shock protein (sHsp) system, which underwent simplification within *Enterobacterales* (which include common bacteria species like *Escherichia coli, Salmonella enterica* and *Erwinia amylovora)* as a model (Fig. 1A).

sHsps are a family of ATP – independent molecular chaperones present in all living organisms with various copy numbers (ten representatives in human)(Haslbeck & Vierling, 2015). They bind misfolded proteins and sequester them into refolding – prone assemblies, preventing uncontrolled aggregation and helping to maintain proteostasis at stress conditions. sHsp are composed of a highly conserved α–crystallin domain (ACD), in a form of so-called β–sandwich, flanked by less conserved, unstructured N – and C – terminal regions (Haslbeck & Vierling, 2015; Haslbeck *et al*, 2019; Reinle *et al*, 2022). Their smallest functional unit is usually a dimer, formed by the interaction between ACDs of two neighboring sHsps. Stable sHsp dimers in turn tend to form variable and dynamic higher – order oligomers, stabilized by N – and C – terminal region interactions**.** Particularly the interaction between IXI motif, highly conserved in sHsps C-termini, and the cleft formed by β4 and β8 strands of ACD is critical for oligomer formation (Haslbeck & Vierling, 2015; Kennaway *et al*, 2005; Mani *et al*, 2016; Strozecka *et al*, 2012). Oligomers of bacterial sHsps reversibly dissociate into smaller forms when the temperature increases. It is considered their activation mechanism, probably uncovering substrate interaction sites. The mechanism of sHsps' interaction with misfolded substrates is not yet fully understood, but both N - termini and β4 – β8 cleft region have been found to play a role in this process (Basha *et al*, 2006; Fuchs *et al*, 2009; Jaya *et al*, 2009; Lee *et al*, 1997; Reinle *et al.*, 2022).

In most *Enterobacterales* a two-protein sHsps system exists, consisting of IbpA and IbpB proteins (Mogk *et al*, 2003; Obuchowski *et al*, 2019). IbpA and IbpB have originated via duplication, form a heterodimer

partnership and are functionally divergent from one another (Obuchowski *et al.*, 2019; Pirog *et al*, 2021) (Fig. 1A,B). IbpA is specialized in tight substrate binding (sequestrase activity), while IbpB is required for dissociation of both sHps from the aggregates, a step necessary to initiate Hsp70-Hsp100 dependent substrate disaggregation and refolding (Obuchowski *et al*, 2021; Ratajczak *et al*, 2009). In a subset of *Enterobacterales* (*Erwiniaceae*), as a result of *ibpB* gene loss, the secondarily single-protein sHsp (IbpA) system has emerged (Fig. 1A,B) (Obuchowski *et al.*, 2019). How did IbpA evolve to become independent of its partner? In this study, using ancestral reconstruction, we identify mutations, which allowed the secondarily single IbpA to be fully functional without its partner in substrate sequestration and handover to Hsp70-Hsp100-mediated disaggregation and refolding.

Results

New activity of *Erwiniaceae* IbpA has evolved in parallel to *ibpB* gene loss

To better understand the evolution of sHsps after gene loss, we reconstructed the IbpA ancestors from before and after the loss of its IbpB partner. This technique uses multiple sequence alignments of modern-day proteins from different species to infer amino acid sequences of its common ancestors (Ashkenazy *et al*, 2012; Pupko *et al*, 2002) and is widely used to investigate various evolutionary questions (Gaucher *et al*, 2008; Longo *et al*, 2020; Thomson *et al*, 2005; Thornton *et al*, 2003). We created a multiple sequence alignment of 77 IbpA sequences from *Enterobacterales*, from which we inferred the phylogeny of IbpA using maximum likelihood method (Fig. S1). From that we inferred ancestral sequences, which have the highest probability of producing the modern-day sequences using the empirical Bayes method (Ashkenazy *et al.*, 2012; Cohen & Pupko, 2011; Cohen *et al*, 2008; Pupko *et al.*, 2002; Simmons & Ochoterena, 2000). Next, we resurrected (i.e., expressed and purified) the last ancestor of IbpA present before ($AncA_0$) and after ($AncA_1$) the differential gene loss (Fig. 1A).

Similarly to modern-day IbpA proteins, both $AncA_0$ and $AncA_1$ were fully folded, and reversibly deoligomerized into smaller species under elevated temperature (Fig. S2). Moreover, both ancestral proteins were able to sequester aggregating firefly luciferase in sHsp-substrate assemblies. $AncA_0$ exhibited sequestrase activity on the level comparable to IbpA from *Escherichia coli* ($IbpA_{E.coli}$). $AncA_1$ was moderately efficient in this process and IbpA from *Erwinia amylovora* ($IbpA_{E.amyl}$) was the least efficient sequestrase (Fig. 1D). Next, we tested their ability to bind protein aggregates in real time (Fig. 1C). Ancestral proteins' interaction with the aggregated substrates was stronger than in the case of extant *E. amylovora* IbpA, but weaker than in the case of extant *E. coli* IbpA (Fig. 1C).

Finally, we asked how the modification of the substrate aggregation process by reconstructed proteins influences subsequent substrate refolding by the Hsp100 and Hsp70 chaperones. $AncA_1$ stimulated luciferase refolding, however its effectiveness was around half of both analyzed extant sHsp systems (single IbpA from *E. amylovora* or IbpA + IbpB system from *E. coli*). $AncA_0$, in contrast, inhibited luciferase refolding in comparison to control (no sHsps at substrate aggregation step) (Fig. 1E).

To test the robustness of our observations, we repeated the analysis for the alternative ancestors, which have the second highest probability to produce the modern-day sequences (AltAll) (Eick *et al*, 2017). Both AltAll variants behaved similarly to most likely (ML) variants in reversible deoligomerization, sequestrase activity and stimulation of substrate refolding assays (Fig. S3A-D). However, the last property (the influence on refolding) required higher Hsp70 system concentration to observe AltAll variants activity (Fig. S3C-D). Together, these data show that reconstructed ML and AltAll ancestors are functional. What is of particular interest, these data clearly point out that the ability of reconstructed sHsps to stimulate Hsp70-Hsp100-dependent substrate refolding arose between A_0 and A_1 nodes.

We performed a molecular evolution analysis to test for positive selection across IbpA phylogeny using both branch models and branch-site models in codeml (Jeffares *et al*, 2015; Yang, 1998, 2007; Yang & Nielsen, 2002). The analysis shows a significantly increased ratio of nonsynonymous to synonymous substitutions, after the gene loss, at the branch leading to A_1 with both tests. This result indicates that the new IbpA functionality likely arose due to an episode of positive selection rather than genetic drift (Figs. 2A, Tables S1, S2). The result of the branch-site test indicates possible positive selection acting on all sites substituted at the branch leading to A_1 with pp>0.5, therefore we aimed to identify minimum number of mutations that are responsible for a change in functional properties of IbpA.

Identification of residues defining ancestral sHsps activities

In order to identify amino acids responsible for the observed new functionality of $AncA_1$, we compared the sequences of two ancestral proteins, selecting seven out of ten substitutions as probable candidates. Three substitutions were removed from analysis based on the low conservation of these positions in extant proteins (Fig. S4). Remaining seven were introduced into $AncA_0$. Resulting $AncA_0$+7 protein stimulated Hsp70-Hsp100-dependent luciferase refolding at the level comparable to $AncA_1$ (Fig. 2B). To further specify key mutations, we prepared seven additional variants. In each variant a different position in $AncA_0$+7 was reversed to a more ancestral state. The substantial decrease in luciferase refolding stimulation was observed for positions 66 and 109 (Fig. 2B). Next, each of these substitutions on its own

(Q66H or G109D) was separately introduced into $AncA_0$. This was not sufficient to increase $AncA_0$ ability to stimulate luciferase refolding. However, when both substitutions were introduced simultaneously, the resulting sHsp exhibited activity similar to $AncA_1$ (Fig. 2C). What is more, when in $AncA_1$ these two positions were reversed to $AncA_0$-like state, the resulting sHsp lost the ability to stimulate luciferase refolding (Fig. 2C). All analyzed proteins, namely $AncA_0$+7, $AncA_0$ Q66H G109D and $AncA_1$ H66Q D109G, possess biochemical properties characteristic for sHsps, exhibiting reversible thermal deoligomerization and sequestrase activity (Fig. S5A-B). All these results show that substitutions Q66H and G109D are both sufficient and necessary for the increase in activity observed for ancestral sHsps between A_0 and A_1 nodes.

Identified substitutions influence α-crystallin domain properties

Substitutions Q66H and G109D, responsible for gaining single sHsp activity, are located in the α-crystallin domain (ACD) within β4 and β8 strands, which form a cleft responsible for the interaction with unstructured C-terminal peptide of the neighboring sHsp dimer (Fig. 3A). In order to identify possible structural underpinnings of the single sHsp activity we have predicted structures of $AncA_0$ and $AncA_0$ Q66H G109D α-crystallin domain (ACD) dimers in complex with C-terminal peptide using AlphaFold2 and subjected them to 0.5 μs equilibrium molecular dynamics (MD) simulations. Analysis of the C-terminal peptide interface contact probabilities in MD trajectories showed that both substituted residues contact the C-terminal peptide, although overall contact pattern remain similar upon their introduction (Fig. S6). To explore the possibility that identified substitutions affect strength of this interaction, we analyzed binding of purified ACDs of $AncA_0$ and $AncA_0$ Q66H G109D to C–terminal peptide using biolayer interferometry. Titrations of immobilized C-terminal peptide by different ACDs (Figs. 3B, S7) allowed us to determine the dissociation constants. These two substitutions increased the K_D of ACD binding to the C -terminal peptide from 4.5 μM to 7.1 μM, indicating a modest decrease in affinity.

As this interaction is known to play a crucial role in formation of sHsp oligomers (Fu *et al*, 2005; Mani *et al.*, 2016; Strozecka *et al.*, 2012), we used dynamic light scattering to investigate how Q66H and G109D substitutions influence the size of oligomers formed by $AncA_0$ at different temperatures. In agreement with decreased affinity between ACD and the C–terminal peptide, we have shown that these substitutions slightly decrease the oligomer size and facilitate $AncA_0$ deoligomerization (Fig. S8A,B).

β4-β8 cleft in certain sHsps, in addition to its interaction with C – terminal peptide, was also shown to participate in interactions with substrates and partner proteins (Fuchs *et al.*, 2009; Jaya *et al.*, 2009; Lee *et al.*, 1997; Reinle *et al.*, 2022). Therefore, we tested whether ACD of $AncA_0$ binds protein aggregates and

whether this interaction is influenced by Q66H G109D substitutions. We observed that $AncA_0$ ACD efficiently binds to either aggregated *E. coli* lysate or aggregated luciferase, and this binding was weakened by analyzed substitutions (Figs. 3C, S9A). This suggests that ACD of bacterial sHsps interacts with the substrate, most likely through the β4-β8 cleft.

These results allow us to conclude that substitutions Q66H and G109D in $AncA_0$ substantially increased the sHsp ability to stimulate Hsp70-Hsp100-dependent substrate refolding by weakening the interaction of β4-β8 cleft with both the C-terminal peptide and the aggregated substrates. Despite its ability to bind aggregated substrates in biolayer interferometry assay, analyzed ACDs do not exhibit sequestrase activity and were unable to positively influence substrate refolding by the Hsp70-Hsp100 system (Fig. S8B-C).

Identified substitutions define the mode of action of extant sHsps

As more ancestral, $AncA_0$-like state in positions 66 and 109 is conserved in IbpA of *E. coli* while more modern, $AncA_1$-like state is conserved in IbpA of *E. amylovora*, we decided to ask whether this difference is sufficient to explain functional differences between the two extant proteins. Therefore, we introduced $AncA_1$-like substitutions into $IbpA_{E.coli}$ and $AncA_0$-like substitutions into $IbpA_{E.amyl}$. Resulting $IbpA_{E.coli}$ Q66H G109D, in comparison to wild type $IbpA_{E.coli}$, exhibited increased ability to stimulate Hsp70-Hsp100-dependent luciferase refolding, as well as a decreased ability to bind aggregated luciferase – becoming more similar to modern *E. amylovora* IbpA. At the same time, $IbpA_{E.amyl}$ H67Q D110G significantly less efficiently stimulated luciferase refolding, while exhibiting increased ability to bind aggregated luciferase in comparison to wild type $IbpA_{E.amyl}$ (Fig. 4A-C). Still, both new IbpA variants exhibited properties characteristic for sHsps, namely reversible thermal deoligomerization and sequestrase activity (Fig. S10A,B).

Above results suggest that tight sHsp binding to aggregates negatively affects subsequent Hsp70-Hsp100-dependent substrate refolding process. It is initiated by binding of the Hsp70 system (DnaK and cochaperones DnaJ and GrpE) to aggregates that requires sHsps to be outcompeted from aggregates (Zwirowski *et al*, 2017). To gain insight into the competition between sHsps and Hsp70 we modified the biolayer interferometry experiments and introduced the sensor with sHsps bound to luciferase aggregates into a buffer containing Hsp70 system (Fig. 4D). Although biolayer interferometry cannot distinguish between proteins bound to the sensor, we took advantage of the differences in the thickness of the protein layers specific for sHsp or Hsp70 binding and also in the binding kinetics. The analysis of the Hsp70 binding to the aggregates covered with sHsps clearly shows that the presence of $IbpA_{E.amyl}$ or $IbpA_{E.coli}$ Q66H

G109D on aggregates only weakly inhibits Hsp70 binding (Fig. 4E,H). In contrast, the inhibition is much more pronounced when $IbpA_{E.amyl}$ H67Q D110G or $IbpA_{E.coli}$ are present on aggregates (Fig. 4F,G).

All above experiments indicate that two specific amino acids in positions 66 and 109 in ACD of IbpA proteins define the mode of IbpA activity. Glutamine 66 and glycine 109 are characteristic for IbpA proteins which bind tightly to substrates and thus are not easily outcompeted from the aggregates by Hsp70s. Such IbpAs require IbpB partner cooperation to function properly. Substitutions at these positions to histidine (position 66) and aspartic acid (position 109) allowed for the emergence of a single sHsp which binds to aggregating substrate less tightly and can be outcompeted from the aggregates by Hsp70s in the absence of IbpB.

Discussion

In this study we traced, at the molecular level, how the two-protein sHsp system, a part of the cellular protein refolding machinery, underwent simplification in a way that its biochemical functions are performed by a single protein. In most *Enterobacterales* two sHsps (IbpA and IbpB) drive sequestration of misfolded proteins into the reactivation-prone assemblies (Obuchowski *et al.*, 2019). Together, IbpA and IbpB form a functional heterodimer, in which IbpA specializes in substrate binding, preventing the substrates from creating large aggregates (sequestrase activity), while IbpB promotes sHsps dissociation from the aggregates required for subsequent Hsp70-Hsp100-dependent substrate refolding (Obuchowski *et al.*, 2019; Pirog *et al.*, 2021). We showed that, in parallel to the *ibpB* gene loss in *Erwiniaceae*, new functions of IbpA have emerged, i.e. a lower substrate sequestrase activity, which correlates with the efficient substrate refolding. We have identified two amino acid substitutions (Q66H and G109D) responsible for this new IbpA functionality. Selection analysis shows that these two substitutions were likely driven by positive selective pressure. This indicates that this change had an adaptive character in the ancestral background, rather than occurring as a result of genetic drift and enabling later loss of *ibpB* gene. Functional differences observed between modern-day sHsps from *E. coli* and *E. amylovora* are at least partially defined by presence of specific amino acids in these two positions and can be diminished by their swapping between extant proteins. Their occurrence in the last common ancestor of *Erwiniaceae* IbpA resulted in a decreased affinity of ACD's β4-β8 cleft to aggregated substrates as well as to the C–termini of the other sHsps. These interactions might be of particular importance for stabilization of sHsps on a surface of sequestered aggregated substrates leading to the formation of so-called protective shell preventing further uncontrolled aggregation. Apparent role of C-termini and ACD interaction is in

agreement with earlier studies, showing that addition of free C-terminal peptide causes *E. coli* IbpA and IbpB dissociation from the outer shell of sHsp - substrate complex (Zwirowski *et al.*, 2017). It was also shown that, in case of Hsp 16.6 from cyanobacterium *Synechocystis*, substitutions that slightly weakened interaction between ACD and C-termini lead to increased stimulation of luciferase refolding. However, abolishing this interaction resulted in a non-functional protein, most likely due to the loss of the sequestrase activity (Giese & Vierling, 2002). Destabilization of the protective shell of secondarily single IbpA by weakening these interactions had an effect functionally analogous to a role of IbpB in the two-protein system, facilitating IbpA dissociation from the substrate (Obuchowski *et al.*, 2019). Two identified substitutions also weaken the ACD interaction with aggregated substrates which is an additional factor shifting the sHsps balance towards dissociation, a step necessary to initiate Hsp70-Hsp100 dependent disaggregation and refolding.

Our results show how ACD substitutions can fine-tune sHsp system by exerting pleiotropic effects on ACD - C-terminal peptide and ACD - substrate interactions. These relatively small changes strongly influence the effectiveness of sHsp functioning in complex process of aggregated protein rescue by molecular chaperones. It might be particularly important in the case of a conserved interaction, like the one between C - terminal peptide and ACD, when excessive changes of affinity may be detrimental to the overall protein function (Giese & Vierling, 2002). Our approach enabled us to find functional residues in sHsp system, which would not have been possible by using conventional mutagenesis and highlights the importance of using vertical approach in biochemical studies. This study closely follows the evolutionary process, in which adaptive mutations in one of the two cooperating proteins tinker it to a point it becomes independent of its partner, enabling the simplification of a more complex system by partner loss while maintaining its overall function.

Following, with molecular precision, the genetic events associated with the gene loss allowed us to answer several questions about protein family evolution. The first question concerns how the lost function is incorporated into a remaining partner protein. The results of our experiments indicate that even though the primary function of a partner protein is maintained, it is altered so that it does not interfere with the newly incorporated one. In our case substrate binding properties, as well as formation of higher-order oligomers were altered in a way to keep the sequestrase function maintained but allow for more efficient stimulation of Hsp70-Hsp100-dependent substrate refolding. The second question concerns the context-dependence of mutations in protein evolution. We successfully transplanted the mutations that appeared in *E. amylovora* into *E. coli* IbpA ortholog, artificially creating an efficient single protein system

from a protein that normally needs a partner for efficient substrate refolding. In contrast to other studies (Natarajan *et al*, 2023) the context of *E.coli* IbpA protein did not influence the ability of $IbpA_{E.coli}$ Q66H G109D to work without IbpB partner. This brings the question about the accessibility of adaptive solutions. In case of *E.coli* IbpA there was no need for adaptive changes because the gene loss did not occur in this clade, suggesting that the loss of a protein can push another one towards an adaptation, which leads to finding efficient molecular innovations.

Materials and Methods

Reconstruction of IbpA phylogeny.

Amino acid sequences of 77 IbpA orthologs from *Enterobacterales* were obtained from NCBI and UniProt databases and aligned using Clustal Omega (Sievers *et al*, 2011). Alignment was trimmed manually. JTT+R3 was identified as the best fit model by iq-tree, using Bayesian Information Criterion and was used in the analysis (Kalyaanamoorthy *et al*, 2017; Nguyen *et al*, 2015). The phylogenetic tree was inferred using iq-tree on the basis of 328 iterations of ML search with 100 rapid bootstraps replicates (Nguyen *et al.*, 2015).

Reconstruction of ancestral IbpA amino acid sequences.

Ancestral sequence reconstruction was performed on the basis of multiple sequence alignment of 77 amino acid sequences of IbpA orthologs from *Erwiniaceae* and *Enterobacreriaceae* as well as a phylogenetic tree of those orthologs (see above). Marginal reconstruction of ancestral sequences was performed with FastML program based on ML algorithm and Bayesian approach using JTT substitution matrix with gamma parameter (Ashkenazy *et al.*, 2012; Cohen & Pupko, 2011; Cohen *et al.*, 2008; Jones *et al*, 1992; Pupko *et al.*, 2002; Simmons & Ochoterena, 2000).

Alternative ancestral sequences for $AncA_0$ and $AncA_1$ proteins were obtained by substituting most likely amino acid on every uncertain position (defined as a position with more than one amino acid with posterior probability ≥ 0.2) with the amino acid with the second highest posterior probability (Eick *et al.*, 2017).

Analysis of natural selection

Analysis of natural selection was performed using codeml. First, Pal2Nal was used to obtain codon alignment based on the multiple sequence alignment of amino acid sequences of IbpA orthologs from *Enterobacterales* (see above) as well as corresponding nucleotide sequences obtained from NCBI database. Resulting codon alignment was then trimmed manually and used together with the phylogenetic tree obtained earlier (see above) for the selection analysis.

For branch model analysis, models M0 (null hypothesis) and Two – ratio (with either $AncA_0$-$AncA_1$ branch or *Erwiniaceae* clade as foreground) were used. For branch – site model analysis, models A null (null hypothesis) and A were used, with foreground branches selected as above. Statistical significance of different models was estimated with Likelihood Ratio Test (LRT) (Jeffares *et al.*, 2015; Yang, 1998, 2007; Yang & Nielsen, 2002).

Protein Purification

Purification of IbpA proteins. pET3a plasmids containing *ancA$_0$, ancA$_1$, ancA$_0$+7, ancA$_{0\,alt_all}$, ancA$_{1alt_all}$* and *ibpA$_{Ea}$* genes were ordered from GeneScript. Point mutations were introduced using site - directed mutagenesis and confirmed by sequencing. Proteins were overproduced in *E. coli* BL21(DE3). Cells were then lysed by sonication in Qsonica sonicator (13% amplitude, 2 min 30 s process time, 15 s pulse-ON time, 45 s pulse-OFF time) in lysis buffer L1 (50 mM Tris pH 7.5, 50 mM NaCl, 5 mM EDTA, 10 % glycerol, 5mM β-mercaptoethanol). Insoluble fraction containing proteins of interest was separated by centrifugation (75 000 x g, 30 min, 4°C) and resolubilized in buffer A (40 mM Tris pH 7.5, 50 mM NaCl, 10% glycerol, 5 mM β-mercaptoethanol, 6M urea) and then centrifuged (75 000 x g, 30 min, 4°C). Supernatant was loaded on Q – Sepharose chromatography column equilibrated with buffer A and eluted in 50 mM - 500 mM NaCl gradient. Fractions containing proteins of interest were then dialyzed to buffer B (40 mM Tris pH 8.5, 50mM NaCl, 10% glycerol, 5mM β-mercaptoethanol) and loaded on Q – Sepharose chromatography column equilibrated with buffer B. Flow-through fraction was collected and dialyzed to buffer C (50 mM Tris pH 7.5, 150 mM KCl, 5% (v/v) glycerol, 5 mM β-mercaptoethanol).

Purification of ACD domains. ACDs of IbpA$_{Ec}$, AncA$_0$ and AncA$_0$ Q66H G109D were purified as described previously (Pirog *et al.*, 2021) and as a final step dialyzed to buffer G (50 mM Tris pH 7.5, 150mM KCl, 5mM β-mercaptoethanol).

Purification of His$_6$–SUMO-C-terminal peptide of AncA$_0$ construct. pET28a plasmid containing gene encoding His$_6$–SUMO fused with C-terminal peptide of AncA$_0$ (PEAMKPPRIEIN) was ordered from GeneScript. Proteins were overproduced in *E. coli* BL21(DE3). Cells were then lysed by sonication in Qsonica sonicator (20% amplitude, 2 min process time, 5s pulse-ON time, 10s pulse-OFF time) in lysis buffer L2 (40 mM Tris pH 7.5, 100 mM NaCl, 10 % glycerol, 10 mM imidazole, 2 mM β-mercaptoethanol). Insoluble fractions were separated by centrifugation for 30 min at 70 000 x g and supernatants, containing proteins of interest, were incubated for 1h with Ni-NTA resin equilibrated with buffer L2. Resins were then washed with the buffer D (40 mM Tris pH 7.5, 100 mM NaCl, 10 % glycerol, 40 mM imidazole, 2mM β-mercaptoethanol) Proteins of interest were eluted from the columns with the buffer E (40 mM Tris pH 7.5, 100 mM NaCl, 10 % glycerol, 400 mM imidazole, 2mM β-mercaptoethanol) and then dialyzed to buffer C (as above).

DnaK, DnaJ, GrpE, ClpB and IbpA$_{Ec}$ proteins were purified as described previously (Ratajczak *et al.*, 2009). IbpB$_{Ec}$ protein was purified as described previously (Pirog *et al.*, 2021). His-tagged luciferase used for BLI measurements was purified as described previously (Obuchowski *et al.*, 2019).

Purity of purified proteins was assessed with SDS-PAGE electrophoresis with Coomassie Blue staining. Protein concentrations were measured using Bradford reaction, with Bovine Serum Albumin as a standard. In the case of His$_6$ – SUMO fused with C-terminal peptide of AncA$_0$, concentration was measured with SDS-PAGE electrophoresis with Coomassie Blue staining coupled with densitometric analysis with Bovine Serum Albumin used as a standard.

QuantiLum® Recombinant Luciferase was purchased from Promega. Creatin Kinase from rabbit muscle was purchased from Sigma Aldrich.

Luciferase refolding assay

1,5 µM recombinant firefly luciferase in buffer F (50 mM Tris pH 7.5, 150 mM KCl, 20 mM $MgCl_2$, 2.5 mM DTT) was denatured by incubation for 10 min at 44°C alone or in the presence of 10 µM sHsps (3uM $IbpA_{Ec}$ + 7µM $IbpB_{Ec}$ in the case of two-protein system from *E. coli*). Denatured luciferase was then incubated at 25 °C with Hsp70 system (1 µM DnaK, 0.4 µM DnaJ and 0.3 µM GrpE), 2 µM ClpB, and ATP regeneration system (5 mM ATP, 0.1 mg/ml creatine kinase and 18 mM creatine phosphate). For experiment presented in Fig. S3C-D, higher concentration of the Hsp70 system was used (2 µM DnaK, 0.8 µM DnaJ and 0.6 µM GrpE). At different timepoints luciferase activity was measured with GLOMAX™ 20/20 luminometer, using the Luciferase Assay System from Promega. Results are presented as averages of at least three independent repeats ± standard deviation.

DLS measurements

Dynamic Light Scattering measurements were performed using Malvern Instruments ZetaSizer Nano S instrument, at 40 µl sample volume, scattering angle 173° and wavelength of 633 nm. For every measurement, minimum ten subsequent series of ten 10-s runs were averaged and particle size distribution was calculated by fitting to 70 size bins between 0.4 and 10,000 nm, as previously described (Zwirowski *et al.*, 2017).

For reversible deoligomerization assay, size of oligomers formed by 10 µM sHsps in buffer F (50 mM Tris pH7.5, 150 mM KCl, 20 mM $MgCl_2$, 2.5 mM DTT) were measured by DLS. First measurement was performed at 25°C and then the sample was heated to 44°C, cooled to 25°C, heated to 44°C and cooled to 25°C, with measurements performed after each change in temperature. Results are presented as size distribution by volume.

For measuring influence of substitutions on oligomer formation, size of oligomers formed by either 10 µM $AncA_0$ or 10 µM $AncA_0$ Q66H G109D in buffer F (as above) was measured by DLS at 25, 27, 29, 31, 33, 35, 37, 39, 41, 43 and 45°C. Results were presented as size distribution by intensity (for temperatures 25°C, 35°C and 45°C) or as an average hydrodynamic diameter corresponding to maximum of a dominant peak of size distribution by volume plotted against temperature ± standard deviation.

For assembly formation (sequestrase) assay, 1.5 µM firefly luciferase in buffer F was denatured alone or in the presence of different sHsp concentrations by incubation at 44°C for 10 min. Size of obtained luciferase aggregates was then measured by DLS at 25°C. Results are presented as an average hydrodynamic diameter of measured particles weighted by intensity (Z-average) ± standard deviation.

Biolayer interferometry (BLI) measurements

sHsps interactions with aggregated luciferase or aggregated *E. coli* lysate were measured using Octet ® K2 system. Anchoring layer of his-tagged luciferase was attached to Octet® NTA Biosensors by 5 min incubation in 0.6 mg/ml his-tagged luciferase in denaturing conditions in buffer UF (50 mM Tris pH 7.5, 4.5 M urea, 150 mM KCl, 20 mM $MgCl_2$, 2.5 mM DTT) at room temperature with 350 rpm shaking. Sensors were then incubated for 5 min as above in buffer H (50 mM Tris pH 7.5, 150 mM KCl, 20 mM $MgCl_2$, 5 mM β-mercaptoethanol) to remove urea and unbound luciferase. The protein aggregate was then formed on the sensor by incubation for 10 min in 0,5 mg/ml his-tagged luciferase or 0.2 mg/ml *E. coli* lysate in buffer H at 44°C (in case of the luciferase) or 55 °C (in case of the lysate). Sensors were then again incubated in

buffer H for 5 min at room temperature with 350 rpm shaking to remove excess protein. Sensors with attached aggregate were placed in the Octet® system in H buffer for 60 s baseline measurement and then placed for 1h in 5 µM sHsp solution in H buffer to measure sHsps association. Sensors were then moved for 1h to buffer H to measure protein dissociation. Measurements were performed with 1000 rpm shaking at 44°C (in case of full - length sHsps) or at 25°C (in case of ACDs). Full- length proteins were preincubated at 44°C for 10 min before measurement.

sHsps displacement by Hsp70 system was measured using ForteBio® BLItz. Sensors with attached aggregates were prepared as described above, with buffer F (50 mM Tris pH7.5, 150 mM KCl, 20 mM $MgCl_2$, 2.5 mM DTT) instead of buffer H. Baseline biolayer was measured for 60 s. Sensors were then placed in 5 µM sHsp solution in buffer F, previously preincubated for 10 min at 44°C. sHsps association was measured for 10 min. Sensors were then moved to either buffer F or Hsp70 system in buffer F (0.7 µM DnaK, 0.28 µM DnaJ, 0.21 µM GrpE, 5 mM ATP, 0.1 mg/ml creatine kinase, 18 mM creatine phosphate). Hsp70 system binding and sHsps dissociation were measured for 1h. Measurements were performed at room temperature with 2000 rpm shaking.

ACD interactions with C –terminal peptide were measured using Octet ® K2 system. Octet® NTA Biosensors were placed in buffer C (50mM Tris pH 7.5, 150 mM KCl, 5% glycerol, 5 mM β-mercaptoethanol) and baseline signal was measured for 60 s. Sensors were then placed in 2.5 µM His_6-SUMO-C-peptide solution in buffer C and incubated for 15 min. Surplus His_6-SUMO-C-peptide was then removed by incubation in G buffer for 15 min. Sensors were then moved to ACD solution and association was measured for 48 min. After that, ACD dissociation was measured in buffer G for 10 min. Measurements were performed with 1000 rpm shaking at 25°C. Measurements were performed for different ACD concentrations in triplicates. Biolayer thickness at the end of association stage was corrected for the background binding using control without ACD and converted to fraction bound by dividing each value by the maximal biolayer thickness. To determine dissociation constant fraction bound as a function of logarithm of ACD concentration was fitted to following sigmoid function equation, using SciPy implementation (Virtanen *et al*, 2020) of Levenberg–Marquardt algorithm:

$$f_b = \frac{L}{1 + e^{(-k*(x-K_D))}} + b$$

Where k and L are respectively input and output scaling factors, b represents binding background, K_D is the dissociation constant, and x is a base 10 logarithm of ACD concentration. Standard deviations of K_D estimates were derived from diagonal of optimized parameters covariance matrix.

Molecular Dynamics (MD)

All MD simulations were performed using Gromacs 2019.2 (Van Der Spoel *et al*, 2005) and CHARMM36-jul2021 as a force field (Huang *et al*, 2017). Simulations were performed in the isothermal-isobaric (NPT) ensemble, where temperature was kept at 310 K using v-rescale thermostat (Bussi *et al*, 2007) with a time constant of 0.1 ps and the pressure was held at 1 bar using Parinello-Rahman barostat (Parrinello & Rahman, 1981). Lennard-Jones potential with a cut-off of 1.0 nm was used to describe Van der Waals interactions. Computation of long-range electrostatic interactions was performed using the particle mesh Ewald (PME) method (Essmann *et al*, 1995) with a Fourier grid spacing of 0.12 nm and a real space cutoff of 1.0 nm. Bonds between hydrogen and protein heavy atoms were constrained by P-LINCS (Hess *et al*, 1997) and water molecules geometry was constrained by SETTLE (Miyamoto & Kollman, 1992). Integration

of equations of motion was performed by leap-frog algorithm (Van Gunsteren & Berendsen, 1988) with a time step of 2 fs. Periodic boundary conditions were applied in all dimensions.

The initial conformation of $AncA_0$ ACD - C-terminal peptide complex was predicted by ColabFold implementation (Mirdita *et al*, 2022) of AlphaFold-Multimer (Richard *et al*, 2022) Substitutions Q66H and G109D were introduced to the complex using PyMol Mutagenesis Wizard (http://www.pymol.org). Complexes were then placed in rhombic dodecahedral boxes measuring 10.4 nm in all dimensions and solvated by CHARMM-modified TIP3P water model (Jorgensen *et al*, 1983). Concentrations of sodium and chloride ions were adjusted to 0.15 M and net zero charge of the system. Each system was subjected to 3-step energy minimization protocol, where during the first step protein conformation was constrained, during the second step constraint was reduced to protein backbone only and during the third step positions of all protein heavy atoms were restrained with a force constant of 1000 $kJ*mol^{-1}*nm^{-1}$. Minimized systems were equilibrated for 10 ns while positions of protein backbone atoms were kept constrained, equilibration was then continued without constraints for further 500 ns. The first 100 ns of equilibration was discarded, and the rest was used for ACD – C-terminal peptide contact determination using GetContacts tool (https://getcontacts.github.io/). Contact between interfacial residues was defined as any of the following types of interaction: hydrogen bond, ionic, π-stacking, π-cation or van der Waals between purely hydrophobic residues. The default GetContacts interaction criteria were used for all interaction types except for hydrogen bond detection, where a more stringent 30° cutoff for hydrogen-donor-acceptor angle was used. Contact heatmaps were prepared using seaborn (Waskom, 2021).

Acknowledgements

This work was supported by a grant of the Polish National Science Centre (OPUS 17 2019/33/B/NZ1/00352). We gratefully acknowledge Poland's high-performance Infrastructure PLGrid (HPC Centers: ACK Cyfronet AGH, PCSS, CI TASK, WCSS) for providing computer facilities and support. We thank Drs. Jaroslaw Marszalek and Agnieszka Kłosowska for discussions.

References

Ashkenazy H, Penn O, Doron-Faigenboim A, Cohen O, Cannarozzi G, Zomer O, Pupko T (2012) FastML: a web server for probabilistic reconstruction of ancestral sequences. *Nucleic Acids Res* 40: W580-584 doi: 10.1093/nar/gks498

Basha E, Friedrich KL, Vierling E (2006) The N-terminal arm of small heat shock proteins is important for both chaperone activity and substrate specificity. *J Biol Chem* 281: 39943-39952 doi: 10.1074/jbc.M607677200

Bussi G, Donadio D, Parrinello M (2007) Canonical sampling through velocity rescaling. *Journal of Chemical Physics* 126Artn 014101
10.1063/1.2408420

Cohen O, Pupko T (2011) Inference of gain and loss events from phyletic patterns using stochastic mapping and maximum parsimony--a simulation study. *Genome Biol Evol* 3: 1265-1275 doi: 10.1093/gbe/evr101

Cohen O, Rubinstein ND, Stern A, Gophna U, Pupko T (2008) A likelihood framework to analyse phyletic patterns. *Philos Trans R Soc Lond B Biol Sci* 363: 3903-3911 doi: 10.1098/rstb.2008.0177

Eick GN, Bridgham JT, Anderson DP, Harms MJ, Thornton JW (2017) Robustness of Reconstructed Ancestral Protein Functions to Statistical Uncertainty. *Mol Biol Evol* 34: 247-261 doi: 10.1093/molbev/msw223

Essmann U, Perera L, Berkowitz ML, Darden T, Lee H, Pedersen LG (1995) A Smooth Particle Mesh Ewald Method. *Journal of Chemical Physics* 103: 8577-8593 doi: Doi 10.1063/1.470117

Fernandez R, Gabaldon T (2020) Gene gain and loss across the metazoan tree of life. *Nat Ecol Evol* 4: 524-533 doi: 10.1038/s41559-019-1069-x

Fu X, Zhang H, Zhang X, Cao Y, Jiao W, Liu C, Song Y, Abulimiti A, Chang Z (2005) A dual role for the N-terminal region of Mycobacterium tuberculosis Hsp16.3 in self-oligomerization and binding denaturing substrate proteins. *J Biol Chem* 280: 6337-6348 doi: 10.1074/jbc.M406319200

Fuchs M, Poirier DJ, Seguin SJ, Lambert H, Carra S, Charette SJ, Landry J (2009) Identification of the key structural motifs involved in HspB8/HspB6-Bag3 interaction. *Biochem J* 425: 245-255 doi: 10.1042/BJ20090907

Gaucher EA, Govindarajan S, Ganesh OK (2008) Palaeotemperature trend for Precambrian life inferred from resurrected proteins. *Nature* 451: 704-707 doi: 10.1038/nature06510

Giese KC, Vierling E (2002) Changes in oligomerization are essential for the chaperone activity of a small heat shock protein in vivo and in vitro. *J Biol Chem* 277: 46310-46318 doi: 10.1074/jbc.M208926200

Haslbeck M, Vierling E (2015) A first line of stress defense: small heat shock proteins and their function in protein homeostasis. *J Mol Biol* 427: 1537-1548 doi: 10.1016/j.jmb.2015.02.002

Haslbeck M, Weinkauf S, Buchner J (2019) Small heat shock proteins: Simplicity meets complexity. *Journal of Biological Chemistry* 294: 2121-2132 doi: 10.1074/jbc.REV118.002809

Hess B, Bekker H, Berendsen HJC, Fraaije JGEM (1997) LINCS: A linear constraint solver for molecular simulations. *Journal of Computational Chemistry* 18: 1463-1472 doi: Doi 10.1002/(Sici)1096-987x(199709)18:12<1463::Aid-Jcc4>3.3.Co;2-L

Huang J, Rauscher S, Nawrocki G, Ran T, Feig M, de Groot BL, Grubmüller H, MacKerell AD (2017) CHARMM36m: an improved force field for folded and intrinsically disordered proteins. *Nature Methods* 14: 71-73 doi: 10.1038/nmeth.4067

Iranzo J, Wolf YI, Koonin EV, Sela I (2019) Gene gain and loss push prokaryotes beyond the homologous recombination barrier and accelerate genome sequence divergence. *Nat Commun* 10: 5376 doi: 10.1038/s41467-019-13429-2

Jaya N, Garcia V, Vierling E (2009) Substrate binding site flexibility of the small heat shock protein molecular chaperones. *Proc Natl Acad Sci U S A* 106: 15604-15609 doi: 10.1073/pnas.0902177106

Jeffares DC, Tomiczek B, Sojo V, dos Reis M (2015) A beginners guide to estimating the non-synonymous to synonymous rate ratio of all protein-coding genes in a genome. *Methods Mol Biol* 1201: 65-90 doi: 10.1007/978-1-4939-1438-8_4

Jones DT, Taylor WR, Thornton JM (1992) The rapid generation of mutation data matrices from protein sequences. *Comput Appl Biosci* 8: 275-282 doi: 10.1093/bioinformatics/8.3.275

Jorgensen WL, Chandrasekhar J, Madura JD, Impey RW, Klein ML (1983) Comparison of Simple Potential Functions for Simulating Liquid Water. *Journal of Chemical Physics* 79: 926-935 doi: Doi 10.1063/1.445869

Kalyaanamoorthy S, Minh BQ, Wong TKF, von Haeseler A, Jermiin LS (2017) ModelFinder: fast model selection for accurate phylogenetic estimates. *Nat Methods* 14: 587-589 doi: 10.1038/nmeth.4285

Kempes CP, van Bodegom PM, Wolpert D, Libby E, Amend J, Hoehler T (2017) Drivers of Bacterial Maintenance and Minimal Energy Requirements. *Frontiers in Microbiology* 810.3389/fmicb.2017.00031

Kennaway CK, Benesch JL, Gohlke U, Wang L, Robinson CV, Orlova EV, Saibil HR, Keep NH (2005) Dodecameric structure of the small heat shock protein Acr1 from Mycobacterium tuberculosis. *J Biol Chem* 280: 33419-33425 doi: 10.1074/jbc.M504263200

Lee GJ, Roseman AM, Saibil HR, Vierling E (1997) A small heat shock protein stably binds heat-denatured model substrates and can maintain a substrate in a folding-competent state. *EMBO J* 16: 659-671 doi: 10.1093/emboj/16.3.659

Lever MA, Rogers KL, Lloyd KG, Overmann J, Schink B, Thauer RK, Hoehler TM, Jørgensen BB (2015) Life under extreme energy limitation: a synthesis of laboratory- and field-based investigations. *FEMS Microbiology Reviews* 39: 688-728 doi: 10.1093/femsre/fuv020

Longo LM, Despotovic D, Weil-Ktorza O, Walker MJ, Jablonska J, Fridmann-Sirkis Y, Varani G, Metanis N, Tawfik DS (2020) Primordial emergence of a nucleic acid-binding protein via phase separation and

statistical ornithine-to-arginine conversion. *Proc Natl Acad Sci U S A* 117: 15731-15739 doi: 10.1073/pnas.2001989117

Lynch M, Marinov GK (2015) The bioenergetic costs of a gene. *Proceedings of the National Academy of Sciences* 112: 15690-15695 doi: doi:10.1073/pnas.1514974112

Mani N, Bhandari S, Moreno R, Hu L, Prasad BVV, Suguna K (2016) Multiple oligomeric structures of a bacterial small heat shock protein. *Sci Rep* 6: 24019 doi: 10.1038/srep24019

Mirdita M, Schütze K, Moriwaki Y, Heo L, Ovchinnikov S, Steinegger M (2022) ColabFold: making protein folding accessible to all. *Nature Methods* 19: 679-682 doi: 10.1038/s41592-022-01488-1

Miyamoto S, Kollman PA (1992) Settle - an Analytical Version of the Shake and Rattle Algorithm for Rigid Water Models. *Journal of Computational Chemistry* 13: 952-962 doi: DOI 10.1002/jcc.540130805

Mogk A, Deuerling E, Vorderwulbecke S, Vierling E, Bukau B (2003) Small heat shock proteins, ClpB and the DnaK system form a functional triade in reversing protein aggregation. *Mol Microbiol* 50: 585-595 doi:

Natarajan C, Signore AV, Bautista NM, Hoffmann FG, Tame JRH, Fago A, Storz JF (2023) Evolution and molecular basis of a novel allosteric property of crocodilian hemoglobin. *Curr Biol* 33: 98-108 e104 doi: 10.1016/j.cub.2022.11.049

Nguyen LT, Schmidt HA, von Haeseler A, Minh BQ (2015) IQ-TREE: a fast and effective stochastic algorithm for estimating maximum-likelihood phylogenies. *Mol Biol Evol* 32: 268-274 doi: 10.1093/molbev/msu300

Obuchowski I, Karas P, Liberek K (2021) The Small Ones Matter-sHsps in the Bacterial Chaperone Network. *Front Mol Biosci* 8: 666893 doi: 10.3389/fmolb.2021.666893

Obuchowski I, Pirog A, Stolarska M, Tomiczek B, Liberek K (2019) Duplicate divergence of two bacterial small heat shock proteins reduces the demand for Hsp70 in refolding of substrates. *PLoS Genet* 15: e1008479 doi: 10.1371/journal.pgen.1008479

Parrinello M, Rahman A (1981) Polymorphic Transitions in Single-Crystals - a New Molecular-Dynamics Method. *Journal of Applied Physics* 52: 7182-7190 doi: Doi 10.1063/1.328693

Pirog A, Cantini F, Nierzwicki L, Obuchowski I, Tomiczek B, Czub J, Liberek K (2021) Two Bacterial Small Heat Shock Proteins, IbpA and IbpB, Form a Functional Heterodimer. *J Mol Biol* 433: 167054 doi: 10.1016/j.jmb.2021.167054

Pupko T, Pe'er I, Hasegawa M, Graur D, Friedman N (2002) A branch-and-bound algorithm for the inference of ancestral amino-acid sequences when the replacement rate varies among sites: Application to the evolution of five gene families. *Bioinformatics* 18: 1116-1123 doi: 10.1093/bioinformatics/18.8.1116

Ratajczak E, Zietkiewicz S, Liberek K (2009) Distinct activities of Escherichia coli small heat shock proteins IbpA and IbpB promote efficient protein disaggregation. *J Mol Biol* 386: 178-189 doi: 10.1016/j.jmb.2008.12.009

Reinle K, Mogk A, Bukau B (2022) The Diverse Functions of Small Heat Shock Proteins in the Proteostasis Network. *J Mol Biol* 434: 167157 doi: 10.1016/j.jmb.2021.167157

Richard E, Michael ON, Alexander P, Natasha A, Andrew S, Tim G, Augustin Ž, Russ B, Sam B, Jason Y *et al* (2022) Protein complex prediction with AlphaFold-Multimer. *bioRxiv*: 2021.2010.2004.463034 doi: 10.1101/2021.10.04.463034

Sievers F, Wilm A, Dineen D, Gibson TJ, Karplus K, Li W, Lopez R, McWilliam H, Remmert M, Soding J *et al* (2011) Fast, scalable generation of high-quality protein multiple sequence alignments using Clustal Omega. *Mol Syst Biol* 7: 539 doi: 10.1038/msb.2011.75

Simmons MP, Ochoterena H (2000) Gaps as Characters in Sequence-Based Phylogenetic Analyses. *Systematic Biology* 49: 369-381

Strozecka J, Chrusciel E, Gorna E, Szymanska A, Zietkiewicz S, Liberek K (2012) Importance of N- and C-terminal regions of IbpA, Escherichia coli small heat shock protein, for chaperone function and oligomerization. *J Biol Chem* 287: 2843-2853 doi: 10.1074/jbc.M111.273847

Thomson JM, Gaucher EA, Burgan MF, De Kee DW, Li T, Aris JP, Benner SA (2005) Resurrecting ancestral alcohol dehydrogenases from yeast. *Nat Genet* 37: 630-635 doi: 10.1038/ng1553

Thornton JW, Need E, Crews D (2003) Resurrecting the ancestral steroid receptor: ancient origin of estrogen signaling. *Science* 301: 1714-1717 doi: 10.1126/science.1086185

Van Der Spoel D, Lindahl E, Hess B, Groenhof G, Mark AE, Berendsen HJ (2005) GROMACS: fast, flexible, and free. *J Comput Chem* 26: 1701-1718 doi: 10.1002/jcc.20291

Van Gunsteren WF, Berendsen HJC (1988) A Leap-Frog Algorithm for Stochastic Dynamics. *Mol Simulat* 1: 173-185 doi: 10.1080/08927028808080941

Virtanen P, Gommers R, Oliphant TE, Haberland M, Reddy T, Cournapeau D, Burovski E, Peterson P, Weckesser W, Bright J *et al* (2020) SciPy 1.0: fundamental algorithms for scientific computing in Python. *Nature Methods* 17: 261-272 doi: 10.1038/s41592-019-0686-2

Waskom ML (2021) seaborn: statistical data visualization. *Journal of Open Source Software* 6: 3021 doi: 10.21105/joss.03021

Yang Z (1998) Likelihood ratio tests for detecting positive selection and application to primate lysozyme evolution. *Mol Biol Evol* 15: 568-573 doi: 10.1093/oxfordjournals.molbev.a025957

Yang Z (2007) PAML 4: phylogenetic analysis by maximum likelihood. *Mol Biol Evol* 24: 1586-1591 doi: 10.1093/molbev/msm088

Yang Z, Nielsen R (2002) Codon-substitution models for detecting molecular adaptation at individual sites along specific lineages. *Mol Biol Evol* 19: 908-917 doi: 10.1093/oxfordjournals.molbev.a004148

Zwirowski S, Klosowska A, Obuchowski I, Nillegoda NB, Pirog A, Zieztkiewicz S, Bukau B, Mogk A, Liberek K (2017) Hsp70 displaces small heat shock proteins from aggregates to initiate protein refolding. *Embo Journal* 36: 783-796 doi: 10.15252/embj.201593378

Figure 1

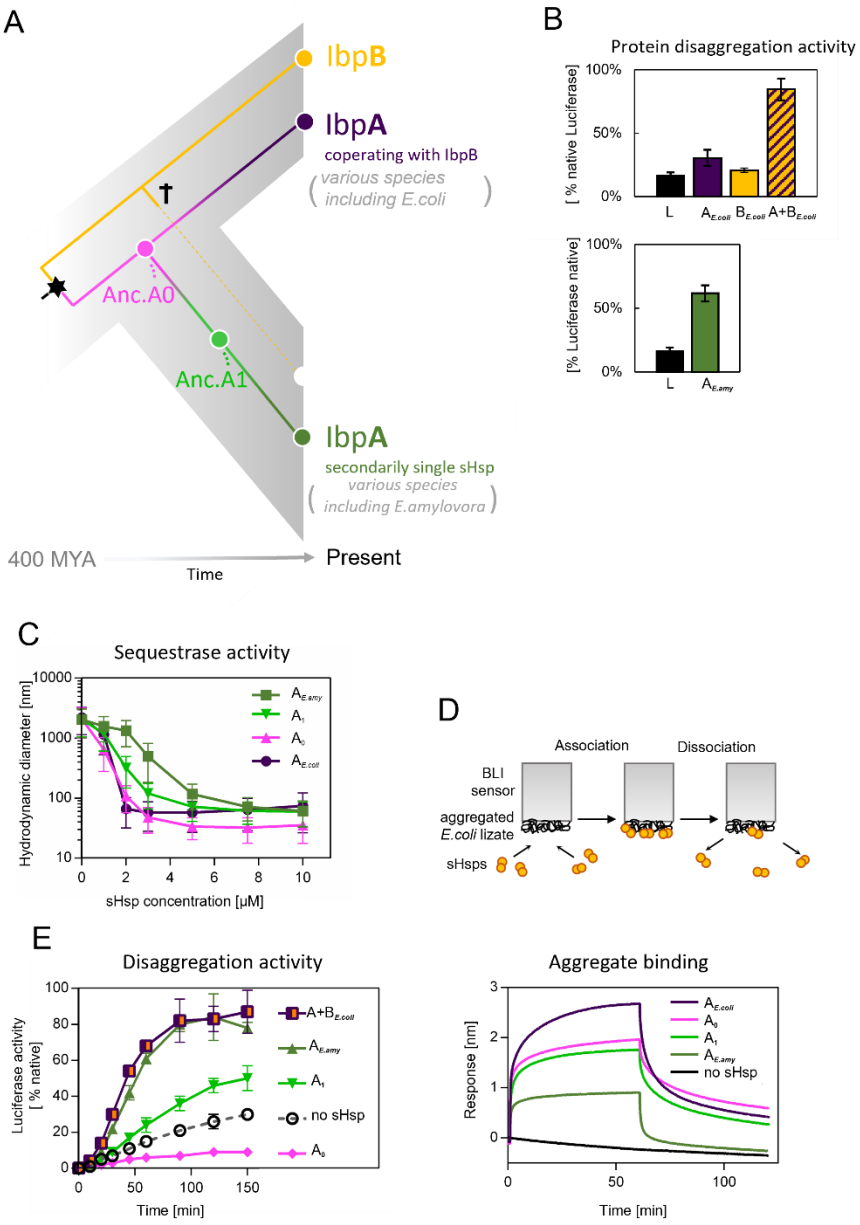

Fig. 1. Functional changes during the evolution of secondarily single sHsp in *Erwiniaceae.* (A) Schematic phylogeny of sHsps in *Enterobacterales*. Gene duplication resulting in IbpA + IbpB two-protein system is marked with a star, while the loss of *ibpB* gene in *Erwiniaceae* clade is marked with a cross; $AncA_0$ – reconstructed last common ancestor of IbpA from *Erwiniaceae* and *Enterobacteriaceae*, expressed as a part of two-protein system; $AncA_1$ – reconstructed last common ancestor of secondarily single IbpA from *Erwiniaceae*. (B) Extant sHsps' ability to stimulate luciferase refolding. sHsps were present during the luciferase thermal denaturation step. Refolding of denatured luciferase was performed by the Hsp70-

Hsp100 chaperone system. (C) Binding of extant and ancestral sHsps to heat-aggregated *E. coli* proteins. *E. coli* proteins were heat aggregated and immobilized on a BLI sensor. sHsps were heat activated before the binding step. (D) Sequestrase activity of extant and ancestral sHsps; Luciferase was heat denatured in the presence of different concentrations of sHsps and size of formed sHsps – substrate assemblies was measured by DLS; results are shown as average hydrodynamic radius ± SD. (E) Extant and ancestral sHsps' ability to stimulate luciferase refolding.

Figure 2

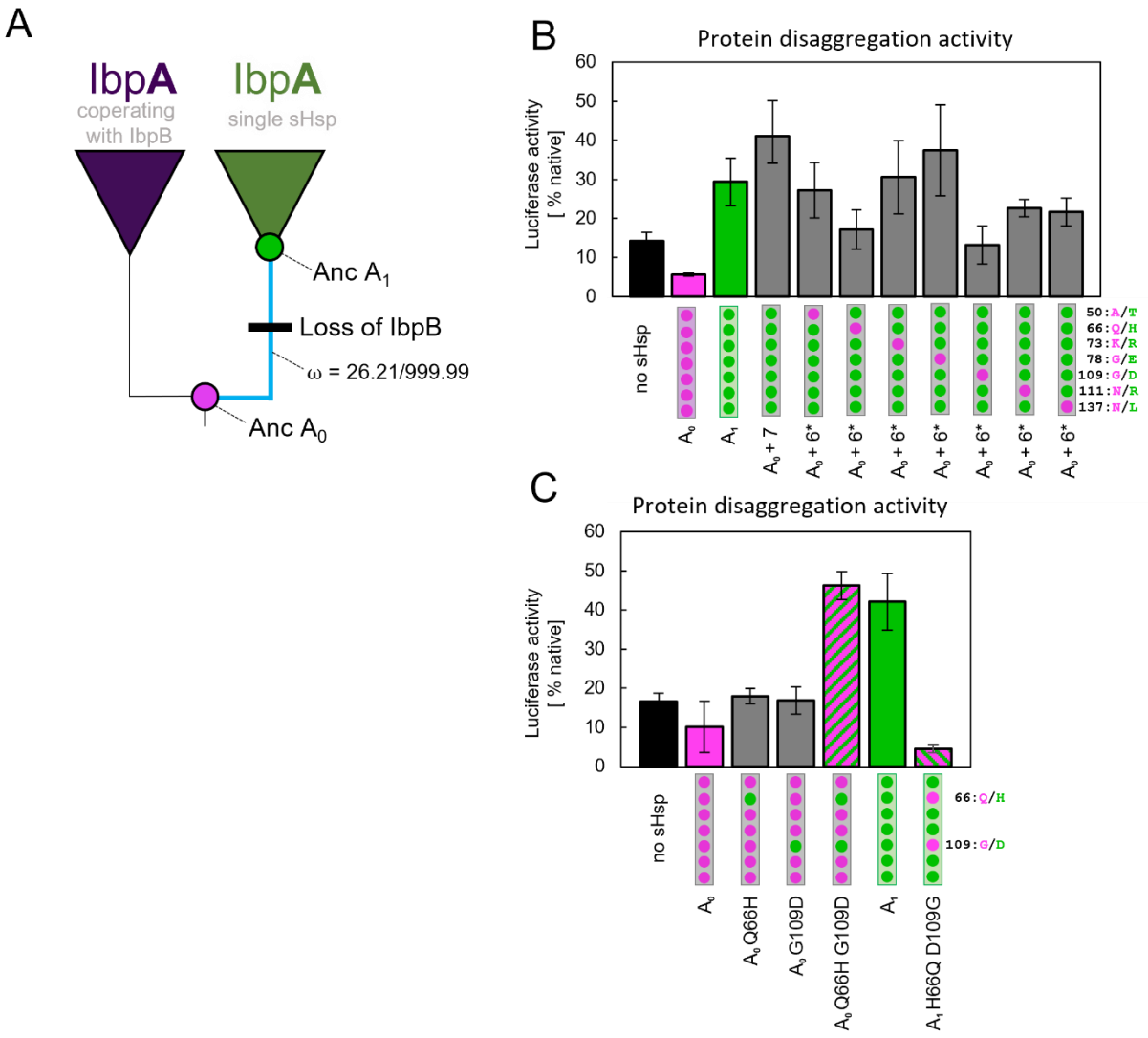

Fig. 2. Substitutions at positions 66 and 109 that occurred between nodes A_0 and A_1 are crucial for ancestral sHsps to work as a single protein. Luciferase refolding assay was performed as in 1B. (A) Schematic phylogeny of *Enterobacterales* IbpA showing increased ratio of nonsynonymous to synonymous substitutions (ω) on the branch between nodes $AncA_0$ and $AncA_1$. Loss of cooperating IbpB

is marked on a tree. (B) Identification of substitutions necessary for $AncA_0$ to obtain $AncA_1$ – like activity in luciferase disaggregation; seven candidate mutations were introduced into $AncA_0$ ($AncA_0$+7); subsequently, in series of six mutants, each of the candidate positions was reversed to a more ancestral state ($AncA_0$ + 6* variants) (C) Effect of substitutions at positions 66 and 109 on the ability of $AncA_0$ and $AncA_1$ to stimulate luciferase refolding.

Figure 3

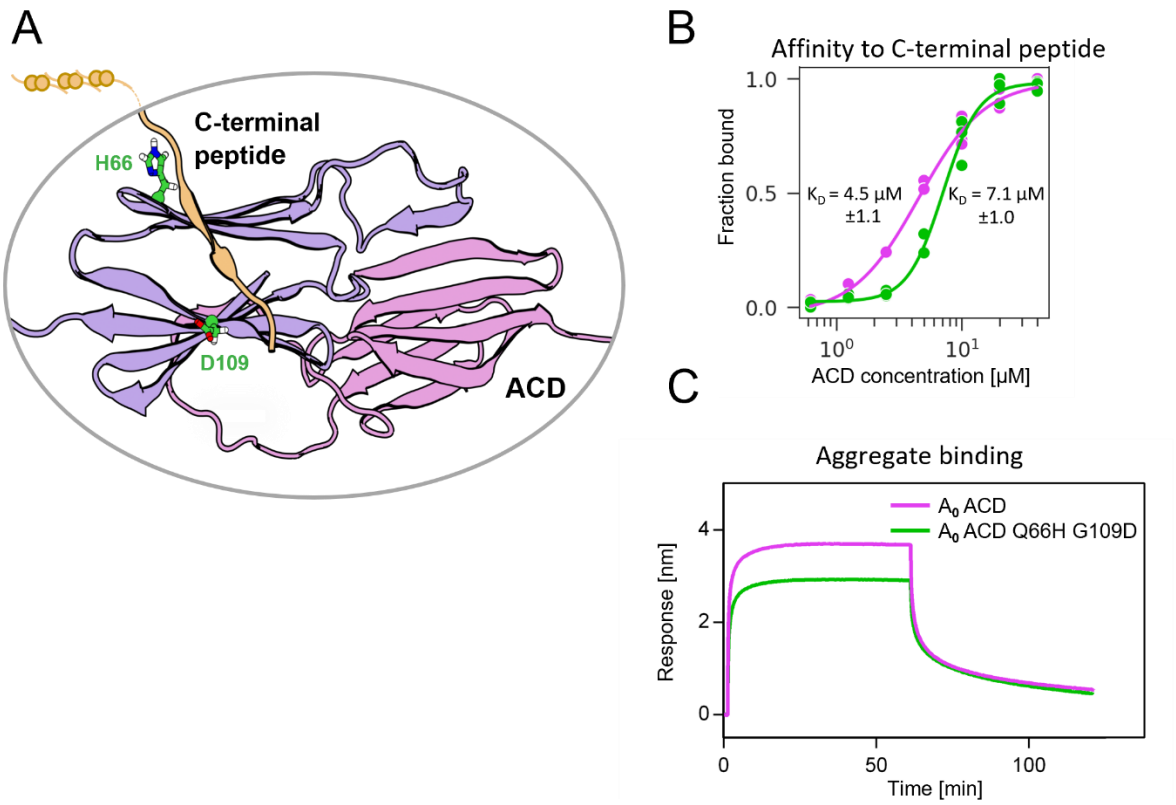

Fig. 3. Substitutions at positions 66 and 109 decreased the affinity of $AncA_0$ ACD to C-terminal peptide and aggregated substrate. (A) Structural model of complex formed by $AncA_0$ Q66H G109D α-crystallin domain dimer (purple and lilac) and $AncA_0$ C-terminal peptide (orange). (B) Effect of Q66H G109D substitutions on $AncA_0$ ACD's affinity to C- terminal peptide. Binding of ACDs of $AncA_0$ or $AncA_0$ Q66H G109D to C-terminal peptide was analyzed by BLI. Biolayer thickness at the end of association step is shown for each concentration as a fraction of thickness at saturating concentration. (C) Effect of Q66H G109D substitutions on $AncA_0$ ACD's affinity to aggregated *E. coli* proteins bound to BLI sensor. Analysis was performed as in 1C.

Figure 4

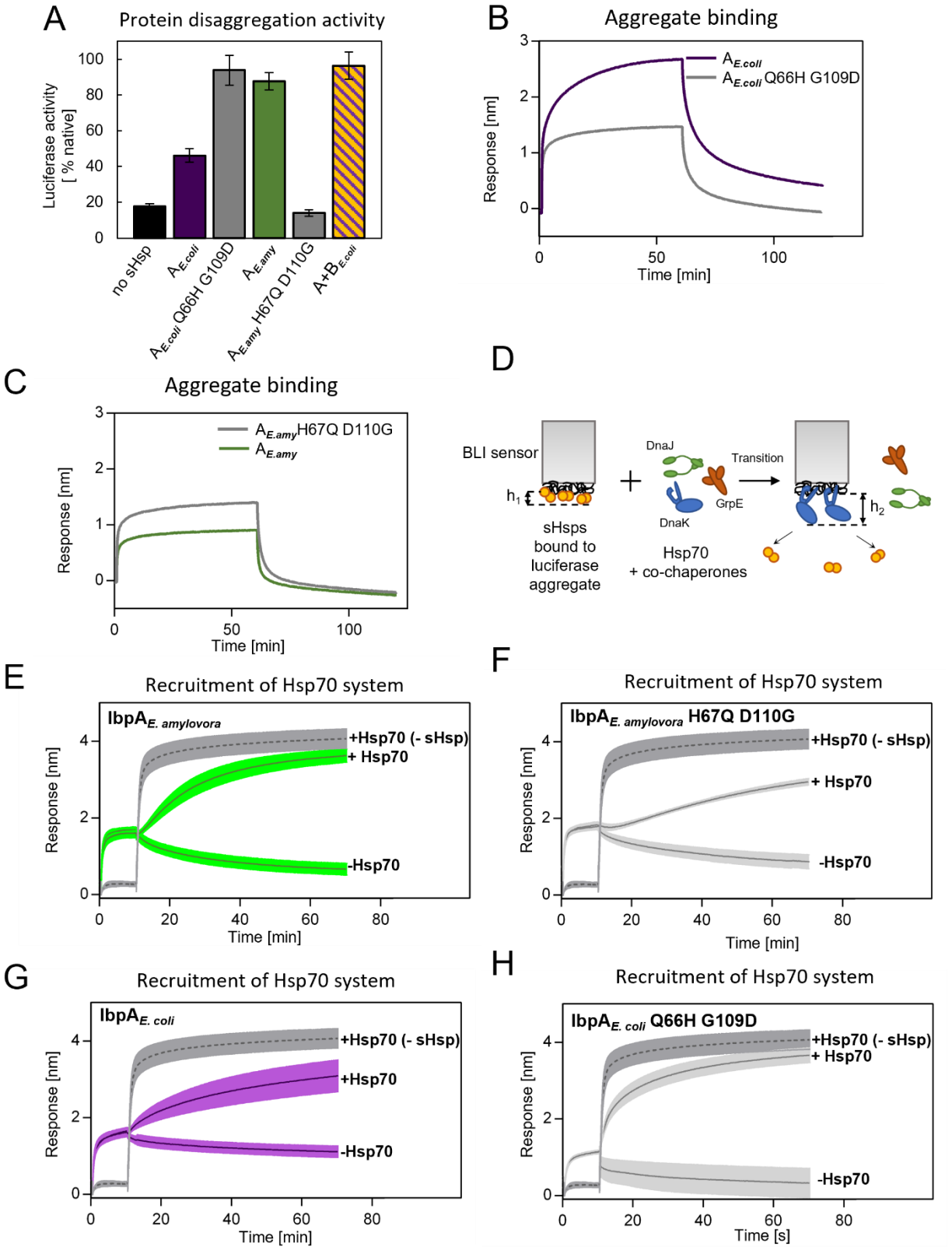

Fig. 4. Differences at positions 66 and 109 determine functional differences between extant IbpA proteins from *E. coli* and *E. amylovora*. (A) Effect of substitutions at position 66 and 109 (and homologous) on the ability of IbpA from E. amylovora and E. coli to stimulate luciferase refolding. Assay was performed as in 1B. (B, C) Effect of substitutions at analyzed positions on binding of IbpA from E. coli (A)and E. amylovora (B) to aggregated luciferase; assay was performed as in 1C. (D-H) Effect of substitutions at analyzed positions on inhibition of Hsp 70 system binding to aggregates by extant sHsps (D) Experimental scheme. (E-H) Aggregate-bound sHsps differently inhibit Hsp70 binding. BLI sensor with immobilized aggregated luciferase and aggregate bound sHsps was incubated with Hsp70 or buffer (spontaneous dissociation curve). Grey traces present Hsp70 binding to immobilized aggregates in the absence of sHsps.